

A Maximum Mass-to-Size Ratio in Scalar-Tensor Theories of Gravity

Tooru TSUCHIDA ^{*} , Go KAWAMURA [†] and Kazuya WATANABE [‡]
Department of Physics, Niigata University, Niigata 950-21, Japan.

Abstract

In this paper, we shall derive a modified Buchdahl inequality in scalar-tensor theories of gravity. In general relativity, Buchdahl has shown that a maximum value of the mass-to-size ratio, $2M/R$, is $8/9$ for static and spherically symmetric stars under some physically reasonable assumptions. We shall apply Buchdahl's method to scalar-tensor theories and obtain theory-independent inequalities as $b/\chi_s \leq 8/9$ and $|c/\chi_s| \leq 2\sqrt{3}/9$, where χ_s is a coordinate radius, and b and c correspond to, up to constant factors, a tensor mass and a scalar mass, respectively. These inequalities are related to a theory-dependent maximum mass-to-size ratio, and we show that its value can exceed not only Buchdahl's limit, $8/9$, but also unity, which we shall call *black hole limit*, in contrast to general relativity. Next, we examine numerically the validity of the assumptions made in deriving the inequalities and the applicability of our analytic results. We find that the assumptions are mostly satisfied and that the mass-to-size ratio exceeds both Buchdahl's limit and a black hole limit. However, we also find that this ratio never exceeds Buchdahl's limit when we impose a further physical assumption, $\rho - 3p \geq 0$, on density, ρ , and pressure, p , of the matter.

1 Introduction

Einstein's general relativity postulates that gravitational interactions are mediated by a tensor field, $g_{\mu\nu}$. It is also well-known that electro-magnetic interactions are mediated by a vector field, A_μ . It is therefore natural to suspect that some unknown interactions may be mediated by scalar fields. Such theories have been suggested since before general relativity. Moreover, it has been repeatedly pointed out over the years that unified theories that contain gravity as well as other interactions, naturally give rise to scalar fields coupled to matter with gravitational strength. This motivation has led many theoretical physicists to study scalar-tensor theories of gravity (scalar-tensor theories) [1],[2],[3],[4]. The scalar-tensor theories are natural alternatives to general relativity, and gravity is mediated not only by a tensor field but also by a scalar field in these theories. Recently, such theories have been of interest as effective theories of the string theory at low energy scales [5].

Many predictions of the scalar-tensor theories in the strong gravitational field are summarized in Ref.[4],[6],[7]. It has been found that a wide class of scalar-tensor theories can pass all the experimental tests in weak gravitational fields. However, it has also been found

^{*}Electronic address:tsuchida@astro2.sc.niigata-u.ac.jp

[†]Electronic address:kawamura@astro2.sc.niigata-u.ac.jp

[‡]Electronic address:kazuya@astro2.sc.niigata-u.ac.jp

that scalar-tensor theories show different aspects of gravity in strong gravitational fields in contrast to general relativity. It has been shown numerically that nonperturbative effects in the scalar-tensor theories increase the maximum mass of an isolated system such as a neutron star[6],[7].

In general relativity, a mass-to-size ratio of a star has physical significance, especially for an isolated system. Buchdahl has obtained a maximum value of the mass-to-size ratio of a static and spherically symmetric star under the following physically reasonable assumptions [8],[9],[10].

- A black hole does not exist.
- Constitution of the star is a perfect fluid.
- The density of the star is a positive and monotonously decreasing function of a radius toward the surface.
- An interior solution of the star smoothly matches the exterior one, i.e., Schwarzschild's solution.

Buchdahl has obtained an upper limit of the mass-to-size ratio as $2M/R \leq 8/9$, which we shall call *Buchdahl inequality*.

Motivated by Buchdahl's theorem, we shall derive a modified Buchdahl inequality to obtain the maximum mass-to-size ratio in scalar-tensor theories. We then examine numerically the validity of the assumptions made in deriving the inequality. The applicability of our analytic results is also examined. This paper is organized as follows. In section 2, we summarize basic equations in the scalar-tensor theories. In section 3, we derive a modified Buchdahl inequality in the scalar-tensor theories, and the numerical results are compared with the analytic results in section 4. A brief summary is given in section 5.

2 Basic equations

We shall consider the simplest scalar-tensor theory [1],[4],[11]. In this theory, gravitational interactions are mediated by a tensor field, $g_{\mu\nu}$, and a scalar field, ϕ . An action of the theory is the following:

$$S = \frac{1}{16\pi} \int \sqrt{-g} \left[\phi R - \frac{\omega(\phi)}{\phi} g^{\mu\nu} \phi_{,\mu} \phi_{,\nu} \right] d^4x + S_{matter}[\Psi_m, g_{\mu\nu}], \quad (2.1)$$

where $\omega(\phi)$ is a dimensionless arbitrary function of ϕ , Ψ_m represents matter fields, and S_{matter} is an action of the matter fields. The scalar field, ϕ , plays a role of an effective gravitational constant as $G \sim 1/\phi$. Varying the action by the tensor field, $g_{\mu\nu}$, and the scalar field, ϕ , yields, respectively, the following field equations:

$$G_{\mu\nu} = \frac{8\pi}{\phi} T_{\mu\nu} + \frac{\omega(\phi)}{\phi^2} \left(\phi_{,\mu} \phi_{,\nu} - \frac{1}{2} g_{\mu\nu} g^{\alpha\beta} \phi_{,\alpha} \phi_{,\beta} \right) + \frac{1}{\phi} (\nabla_\mu \nabla_\nu \phi - g_{\mu\nu} \square \phi), \quad (2.2)$$

$$\square \phi = \frac{1}{3 + 2\omega(\phi)} \left(8\pi T - \frac{d\omega}{d\phi} g^{\alpha\beta} \phi_{,\alpha} \phi_{,\beta} \right). \quad (2.3)$$

Now we perform the following conformal transformation,

$$g_{\mu\nu} = A^2(\varphi) g_{*\mu\nu}, \quad (2.4)$$

such that

$$G_* A^2(\varphi) = \frac{1}{\phi}, \quad (2.5)$$

where G_* is a bare gravitational constant, and we call $A(\varphi)$ *coupling function*. Hereafter, a symbol, $*$, denotes quantities or derivatives associated with $g_{*\mu\nu}$. Then the action is rewritten as

$$S = \frac{1}{16\pi G_*} \int \sqrt{-g_*} (R_* - 2g_*^{\mu\nu} \varphi_{,\mu} \varphi_{,\nu}) d^4x + S_{matter}[\Psi_m, A^2(\varphi) g_{*\mu\nu}], \quad (2.6)$$

where a scalar field, φ , is defined by

$$\alpha^2(\varphi) \equiv \left(\frac{d \ln A(\varphi)}{d\varphi} \right)^2 = \frac{1}{3 + 2\omega(\phi)}. \quad (2.7)$$

Varying the action by $g_{*\mu\nu}$ and φ yields, respectively,

$$G_{*\mu\nu} = 8\pi G_* T_{*\mu\nu} + 2 \left(\varphi_{,\mu} \varphi_{,\nu} - \frac{1}{2} g_{*\mu\nu} g_*^{\alpha\beta} \varphi_{,\alpha} \varphi_{,\beta} \right), \quad (2.8)$$

$$\square_* \varphi = -4\pi G_* \alpha(\varphi) T_*, \quad (2.9)$$

where $T_*^{\mu\nu}$ represents a energy-momentum tensor with respect to $g_{*\mu\nu}$ defined by

$$T_*^{\mu\nu} \equiv \frac{2}{\sqrt{-g_*}} \frac{\delta S_{matter}[\Psi_m, A^2(\varphi) g_{*\mu\nu}]}{\delta g_{*\mu\nu}} = A^6(\varphi) T^{\mu\nu}. \quad (2.10)$$

The conservation law of $T_*^{\mu\nu}$ is given by

$$\nabla_{*\nu} T_{*\mu}^\nu = \alpha(\varphi) T_* \nabla_{*\mu} \varphi. \quad (2.11)$$

The field equations (2.9) and (2.11) tell us that a *coupling strength*, $\alpha(\varphi)$, plays a role in mediating interactions between the scalar field, φ , and the matter. General relativity is characterized by having a vanishing coupling strength: $\alpha(\varphi) = 0$, i.e., $A(\varphi) = 1$. The Jordan-Fierz-Brans-Dicke theory is characterized by having a φ -independent coupling strength: $\alpha(\varphi) = \alpha_0 = \text{const.}$, i.e., $A(\varphi) = e^{\alpha_0 \varphi}$ [1],[6]. Observational constraints on the coupling strength are summarized in Appendix A.

3 Modified Buchdahl's theorem in scalar-tensor theories

In this section, we shall consider a static and spherically symmetric space-time with perfect fluid. First, we derive a modified Buchdahl inequality. Then the inequality is reformulated to obtain a maximum value of the mass-to-size ratio in the scalar-tensor theories. Hereafter, we call $(g_{\mu\nu}, \phi)$ and $(g_{*\mu\nu}, \varphi)$, respectively, physical frame and unphysical frame.

3.1 A modified Buchdahl inequality in scalar-tensor theories

In the unphysical frame, a line element of the static and spherically symmetric space-time is written as [10]

$$ds_*^2 = -f_*(r)dt^2 + h_*(r)dr^2 + r^2d\Omega^2. \quad (3.1)$$

A stress-energy tensor of the perfect fluid in the unphysical frame is given by

$$T_*^{\mu\nu} = (\rho_* + p_*)u_*^\mu u_*^\nu + p_*g_*^{\mu\nu}, \quad u_{*\alpha} = -\sqrt{f_*(r)}(dt)_\alpha, \quad (3.2)$$

where u_*^α is a four velocity of the matter. Fluid variables in the physical and unphysical frames are related as

$$u^\alpha = u_*^\alpha A^{-1}(\varphi), \quad (3.3)$$

$$\rho = \rho_* A^{-4}(\varphi), \quad (3.4)$$

$$p = p_* A^{-4}(\varphi). \quad (3.5)$$

Now the field equations (2.8) and (2.9) are reduced to the following equations:

$$(r(1 - h_*^{-1}))' = 8\pi G_* \rho_* r^2 + \frac{r^2}{h_*} \varphi'^2, \quad (3.6)$$

$$-r^{-2}h_*(1 - h_*^{-1}) + r^{-1}f_*^{-1}f_*' = 8\pi G_* p_* h_* + \varphi'^2, \quad (3.7)$$

$$\left(\frac{f_*'}{2f_*}\right)' + \left(\frac{f_*'}{2f_*}\right)^2 + \frac{1}{r} \frac{f_*'}{2f_*} - \frac{h_*'}{2h_*} \frac{f_*'}{2f_*} - \frac{1}{r} \frac{h_*'}{2h_*} = 8\pi G_* p_* h_* - \varphi'^2, \quad (3.8)$$

$$r^{-2}(f_* h_*)^{-\frac{1}{2}} \left(\left(\frac{f_*}{h_*}\right)^{\frac{1}{2}} r^2 \varphi'\right)' = 4\pi G_* \alpha(\varphi)(\rho_* - 3p_*), \quad (3.9)$$

where a prime denotes a derivative with respect to r . As is often done in the cases of general relativity, we define a *mass function*, $m_*(r)$, in the unphysical frame as follows:

$$h_*(r) \equiv \left[1 - \frac{2m_*(r)}{r}\right]^{-1}. \quad (3.10)$$

Then (3.6) is rewritten as

$$m_*'(r) = 4\pi G_* \rho_{\text{eff}} r^2, \quad (3.11)$$

where

$$\rho_{\text{eff}} \equiv \rho_* + \frac{\varphi'^2}{8\pi G_* h_*}. \quad (3.12)$$

That is, ρ_{eff} plays a role of an effective density in the unphysical frame.

In order to derive a modified Buchdahl inequality, we assume as follows:

$$h_*(r) \geq 0, \quad (3.13)$$

$$f_*(r) \geq 0, \quad (3.14)$$

$$\rho_{\text{eff}}(r) \geq 0, \quad (3.15)$$

$$\rho'_{\text{eff}}(r) \leq 0. \quad (3.16)$$

These assumptions mean

- A black hole does not exist in the unphysical frame.
- The effective density, ρ_{eff} , is a positive and monotonously decreasing function of a radius toward the surface.

Moreover, we assume that an interior solution of the above field equations smoothly matches the exterior one. Note that these assumptions are concerned with the unphysical variables and that their validity should be examined, as will be done later.

Using the assumption (3.16), it is easy to verify the following inequality:

$$\left(\frac{m_*}{r^3}\right)' \leq 0. \quad (3.17)$$

Moreover, with (3.7), (3.8) and (3.11), we obtain the following inequality:

$$-\left(\frac{(\sqrt{f_*})'}{r\sqrt{h_*}}\right)' = \sqrt{f_*h_*}\left(-\left(\frac{m_*}{r^3}\right)' + 2\frac{\varphi'^2}{rh_*}\right) \geq 0. \quad (3.18)$$

Accordingly, we have

$$\frac{\left(\sqrt{f_*(r_1)}\right)'}{r_1\sqrt{h_*(r_1)}} \geq \frac{\left(\sqrt{f_*(r_2)}\right)'}{r_2\sqrt{h_*(r_2)}}, \quad r_1 \leq r_2. \quad (3.19)$$

Now let the inequality (3.19) be reformulated in terms of variables of the exterior solution. The exterior solution, whose derivation is given in Appendix B, is the following:

$$ds_*^2 = -e^{\gamma(x)}dt^2 + e^{-\gamma(x)}d\chi^2 + e^{\lambda(x)-\gamma(x)}d\Omega^2, \quad (3.20)$$

where

$$e^{\lambda(x)} = \chi^2 - a\chi, \quad (3.21)$$

$$e^{\gamma(x)} = \left(1 - \frac{a}{\chi}\right)^{\frac{b}{a}}, \quad (3.22)$$

$$\varphi(x) = \varphi_0 + \frac{c}{a} \ln\left(1 - \frac{a}{\chi}\right), \quad (3.23)$$

where a , b , c , and φ_0 are constants of integration, and φ_0 is an asymptotic value of φ at infinity. Moreover, the constants, a , b and c , must satisfy the following relation (Appendix B):

$$a^2 - b^2 = 4c^2. \quad (3.24)$$

One may expect that $\chi = a$ is an event horizon, however, it is not a case in generic scalar-tensor theories, where the null surface, $\chi = a$, is a curvature singularity in the unphysical frame. The singular nature of the unphysical space-time at $\chi = a$ can also be seen when the transformation to the Schwarzschild coordinate is done. The Schwarzschild coordinate, r , and the Just coordinate, χ , are related by the following relation:

$$r = \chi \left(1 - \frac{a}{\chi}\right)^{\frac{a-b}{2a}}. \quad (3.25)$$

One finds that, when $a \neq b$, $\chi = a$ in the Just coordinate corresponds to $r = 0$ in the Schwarzschild coordinate.

By matching the interior solution to the exterior solution, we obtain the following relations:

$$r_s = \chi_s \left(1 - \frac{a}{\chi_s}\right)^{\frac{a-b}{2a}}, \quad (3.26)$$

$$f_*(r_s) = \left(1 - \frac{a}{\chi_s}\right)^{\frac{b}{a}}, \quad (3.27)$$

$$h_*(r_s) = \left(1 - \frac{a}{\chi_s}\right) \left(1 - \frac{a+b}{2\chi_s}\right)^{-2}, \quad (3.28)$$

where a subscript, s , refers to χ evaluated at the surface, $r = r_s$. Note that

$$\chi \geq \chi_s > a \geq b. \quad (3.29)$$

Since $h_*(r)^{-1} = 1 - 2m_*(r)/r$, (3.28) becomes

$$2m_*(r_s) = \left(b - \frac{(a+b)^2}{4\chi_s}\right) \left(1 - \frac{a}{\chi_s}\right)^{-\frac{(a+b)}{2a}}. \quad (3.30)$$

Accordingly, by virtue of positivity of $m_*(r)$, we obtain an additional inequality:

$$b - \frac{(a+b)^2}{4\chi_s} \geq 0. \quad (3.31)$$

With (3.19) and (3.25) \sim (3.28), we obtain the following relation for $r \leq r_s$:

$$\frac{(\sqrt{f_*})'}{r\sqrt{h_*}} \geq \frac{\left(\sqrt{f_*(r_s)}\right)'}{r_s\sqrt{h_*(r_s)}} = \frac{b}{2r_s^3}. \quad (3.32)$$

Integrating (3.32) from the center, $r = 0$, to the surface, $r = r_s$, we obtain the following inequality:

$$\begin{aligned} 0 &\leq \sqrt{f_*(0)} \\ &\leq \sqrt{f_*(r_s)} - \frac{b}{2r_s^3} \int_0^{r_s} r \sqrt{h_*(r)} dr \\ &\leq \sqrt{f_*(r_s)} - \frac{b}{2r_s^3} \int_0^{r_s} r \left(1 - \frac{2m_*(r_s)}{r_s^3} r^2\right)^{-\frac{1}{2}} dr \\ &= \left(1 - \frac{a}{\chi_s}\right)^{\frac{b}{2a}} + \frac{b}{4m_*(r_s)} \left(\sqrt{1 - \frac{2m_*(r_s)}{r_s}} - 1\right), \end{aligned} \quad (3.33)$$

where the inequality (3.17) is used.

The inequalities obtained so far are simplified in terms of new parameters defined by

$$a_s \equiv \frac{a}{\chi_s}, \quad b_s \equiv \frac{b}{\chi_s}, \quad c_s \equiv \frac{c}{\chi_s}. \quad (3.34)$$

Substituting (3.30) in (3.33), we obtain the following inequality:

$$\begin{aligned} 0 &\leq \sqrt{f_*(0)} \\ &\leq \frac{1}{2}(1-a_s)^{\frac{b_s}{2a_s}} \left(b_s - \frac{(a_s+b_s)^2}{4}\right)^{-1} \times \\ &\quad \times \left[2b_s - \frac{(a_s+b_s)^2}{2} - b_s\sqrt{1-a_s} \left(1 - \sqrt{1 - \frac{4b_s - (a_s+b_s)^2}{4(1-a_s)}}\right)\right]. \end{aligned} \quad (3.35)$$

The above inequality can be further simplified, and we finally obtain a modified Buchdahl inequality in the scalar-tensor theories as

$$F(a_s, b_s) \equiv 3b_s - \frac{1}{2}(a_s + b_s)(a_s + 2b_s) - b_s\sqrt{1 - a_s} \geq 0, \quad (3.36)$$

supplemented with (3.29) and (3.31).

The modified Buchdahl inequality can be solved to find

$$\left. \begin{array}{ll} b_s \leq a_s \leq 2\sqrt{b_s} - b_s & \text{for } 0 \leq b_s \leq 4(3 - 2\sqrt{2}), \\ b_s \leq a_s \leq 2\sqrt{2b_s} - 2b_s & \text{for } 4(3 - 2\sqrt{2}) \leq b_s \leq \frac{8}{9}, \\ \text{Forbidden} & \text{for } b_s \geq \frac{8}{9}. \end{array} \right\} \quad (3.37)$$

Fig. 1 displays the allowed region, D , of (a_s, b_s) .

In addition, we can obtain, with (3.24), an upper limit of $|c_s|$ as follows:

$$|c_s| \leq \frac{2\sqrt{3}}{9}. \quad (3.38)$$

The inequality (3.37) has significant importance. The third inequality of (3.37) tells us a necessary condition for a spherical star to exist and is reduced to Buchdahl's theorem in general relativity when $c = 0$, i.e., $a = b$, and, accordingly, $\chi = r$. In this case, we have ($R = r_s$)

$$c_s = 0 \iff a_s = b_s = \frac{2M}{R} \leq \frac{8}{9}, \quad (3.39)$$

where M is the ADM mass defined at spatial infinity, and R is related to the surface area, S , as $S = 4\pi R^2$.

The new and important inequality (3.38) is characteristic to the scalar-tensor theories and does not have a general relativistic counterpart. It has been found the appearance of nonperturbative behaviors of the scalar field in the previous numerical studies [6],[7]. Our result means that, even in the strong gravitational field, an amplitude of the scalar mass, $M_s \equiv -c/G_*$, is bounded.

It is important to note that we have not used any assumption on the coupling function, $A(\varphi)$, in deriving the inequalities. In particular, the inequalities (3.37) and (3.38) give theory-independent constraints on the parameters, b_s and c_s .

3.2 A mass-to-size ratio

Now we will reformulate the inequalities derived in the previous section, which are in terms of variables in the unphysical frame, in order to obtain a mass-to-size ratio in the physical frame. To do that, a coupling function, $A(\varphi)$, should be specified. In this paper, we take an example of the coupling function in a simple form given by

$$A(\varphi) = e^{\frac{1}{2}\beta\varphi^2}, \quad (3.40)$$

where β is a constant[6],[7]. Then the coupling strength, $\alpha(\varphi)$, becomes

$$\alpha(\varphi) = \beta\varphi. \quad (3.41)$$

A natural definition of a radius of the spherical star is done by using its (physical) surface area as follows. In the physical frame, the surface area, S , is given by

$$\begin{aligned} S &= 4\pi A^2(\varphi_s) e^{\lambda(\chi_s) - \gamma(\chi_s)} \\ &= 4\pi \chi_s^2 (1 - a_s)^{1 - \frac{b_s}{a_s}} \exp \left[\beta \left(\frac{c_s}{a_s} \ln(1 - a_s) \right)^2 \right], \end{aligned} \quad (3.42)$$

where we take an asymptotic value of the scalar field as $\varphi_0 = 0$, and, accordingly, we have $A(\varphi_0) = 1$ and $\alpha(\varphi_0) = 0$. This surface area defines a physical radius, R , of the star in a similar manner as in general relativity:

$$R \equiv \sqrt{\frac{S}{4\pi}}. \quad (3.43)$$

When $\varphi_0 = 0$, an effective gravitational constant, G , defined in Appendix A, is equal to G_* . If $\varphi_0 \neq 0$, contributions of the scalar mass appear in the above expression of R in terms of $c\beta\varphi_0$.

The ADM mass in the physical frame is obtained by the asymptotic expression of g_{00} at spatial infinity:

$$\begin{aligned} -g_{00} &= A^2(\varphi) e^\gamma \\ &= \left(1 - \frac{a}{\chi} \right)^{\frac{b}{a}} \exp \left[\beta \left(\frac{c}{a} \ln \left(1 - \frac{a}{\chi} \right) \right)^2 \right] \\ &\xrightarrow{\chi \rightarrow \infty} 1 - \frac{b}{r} + \mathcal{O} \left(\frac{1}{r^2} \right). \end{aligned} \quad (3.44)$$

Accordingly, $M_T \equiv b/2G$ is the ADM mass.

Now we are ready to calculate a mass-to-size ratio in the scalar-tensor theory as a function of a_s , b_s , χ_s and a specific parameter of our model, β . We obtain

$$H(a_s, b_s; \beta) \equiv \frac{b}{R} = b_s (1 - a_s)^{\frac{b_s - a_s}{2a_s}} \exp \left[-\frac{1}{2} \beta \left(\frac{c_s}{a_s} \ln(1 - a_s) \right)^2 \right]. \quad (3.45)$$

In Fig.2, in the allowed region of (a_s, b_s) , we show lines on which $H(a_s, b_s; \beta)$ is equal to $8/9$ for various values of β . For a fixed value of β , an upper region over the line corresponds to the cases that the mass-to-size ratio, $2M/R$, exceeds Buchdahl's limit, $8/9$. Moreover, in some cases, it may be greater than unity, which we shall call *black hole limit*. The maximum values of $H(a_s, b_s; \beta)$ for various values of β are shown in Fig.3. Indeed, the maximum mass-to-size ratio can sometimes become larger than the black hole limit. However, the physical exterior solution generically does not have an event horizon in scalar-tensor theories in contrast to general relativity, and, therefore, the condition, $2M/R > 1$, does not mean the existence of a black hole. Now suppose that a space rocket approaches such a star and goes into its *Schwarzschild radius* defined by $2M$. A spaceman in the rocket would be resigned to his fate to die, but we know that he still has a chance to return alive from the *false black hole*.

4 Numerical results

We numerically solve (3.6) \sim (3.9) to obtain an interior solution. The solution is then matched to the exterior one, and numerical values of the parameters, a_s , b_s and c_s are calculated. Some details of the numerical methods are summarized in Appendix C. Since we take $\varphi_0 = 0$, G_* is equal to G (Appendix A). Hereafter, we use the unit, $G_* = G = 1$.

As for the matter, we assume the following polytropic equation of state [13]:

$$\rho = m_b n + \frac{Kn_0 m_b}{\Gamma - 1} \left(\frac{n}{n_0} \right)^\Gamma, \quad (4.1)$$

$$p = Km_b n_0 \left(\frac{n}{n_0} \right)^\Gamma, \quad (4.2)$$

$$m_b = 1.66 \times 10^{-24} \text{g}, \quad (4.3)$$

$$n_0 = 0.1 \text{fm}^{-3}. \quad (4.4)$$

We take the parameters, $\Gamma = 2.34$ and $K = 0.0195$ [6], which well fit a realistic equation of state of the high density nuclear matter and probably also that of a neutron star. Our numerical solutions are therefore parametrized by β and $n_c \equiv n(0)$. It has been numerically shown that significant effects of φ appear when $\beta \leq -4.35$ [6],[7], and we are mostly interested in cases of negative values of β . In cases of positive values of β , we cannot find numerically any significantly different behaviors of the solutions compared with those in general relativity, and any further discussion in these cases is no longer done.

First, we examine whether our assumption, $\rho'_{\text{eff}} \leq 0$, is satisfied. In Fig.4, we show an example of numerical behaviors of the effective density for $\beta = -5$ and $n_c/n_0 = 10$. Including this case, we find that the assumption, $\rho'_{\text{eff}}(r) \leq 0$, is mostly satisfied as summarized in the 3rd column of Table 1. By differentiating (3.12), one obtains

$$\rho'_{\text{eff}} = A^4(\varphi)\rho' + 4A^4(\varphi)\alpha(\varphi)\varphi'\rho + \left(\frac{\varphi'^2}{8\pi G_* h_*} \right)', \quad (4.5)$$

In Fig.5, we show the 1st, 2nd and 3rd terms in (4.5) with the same parameters as Fig.4. The first term is indeed dominant and always negative. In Fig.6, we compare the corresponding physical quantities, $\rho(r)$ and $\phi(r)$, and the unphysical scalar field, $\varphi(r)$. It is found that a *local gravitational constant*, $G(\phi) \equiv 1/\phi$, increases as ρ decreases toward the surface. However, this behavior is strongly coupling function-dependent, and a sign of β is crucial in the present case.

Next, we examine an extreme example in which the assumption, $\rho'_{\text{eff}} \leq 0$, is violated. Fig.7 shows the effective density, ρ_{eff} , for $\beta = -30$ and $n_c/n_0 = 10$. It is seen that ρ_{eff} remains constant in the central part and then increases between two rectangles in Fig.7. This peculiar behavior of ρ_{eff} indicates that the star may be in an unusual scalar field-supported equilibrium in contrast to usual pressure-supported stars. In Fig.8, we show the three terms in (4.5) and find that the positive second term becomes partially dominant. Again, this behavior is strongly coupling function-dependent. In the present case, we have $\alpha(\varphi) = \beta\varphi$, where $\beta < 0$. Therefore, when $\varphi' < 0$, and $|\beta|$ is large such that the second term in (4.5) is dominant, ρ'_{eff} becomes positive, and the assumption is violated. In Fig.9, we compare $\rho(r)$, $\phi(r)$ and $\varphi(r)$. It is found that, despite small values of φ , ϕ can be large due to a large value of $|\beta|$. However, it should be noted that the assumption is concerned with the unphysical quantity, ρ_{eff} , and that its violation does not necessarily mean that this extreme case must be unreal. In Fig.10, we show the energy density, $\rho(r)$, and the pressure, $p(r)$, in the physical frame in

the extreme case: $\beta = -30$, $n_c/n_0 = 10$. Behaviors of these quantities seem ordinary, that is, they are monotonously decreasing functions of r . Accordingly, one may think that this can be a physically acceptable equilibrium solution despite the violation of the assumption, $\rho'_{\text{eff}} \leq 0$. However, we are forbidden to take β smaller than -5 because of the experimental constraints (Appendix A, [7],[12]).

For each value of β , the mass-to-size ratio, $2M/R = H(a_s, b_s; \beta)$, can be numerically calculated as a function of n_c . By changing n_c , we search a maximum value of $H(a_s, b_s; \beta)$ for each β . In the 5th column of Table1, we summarize our results of the maximum mass-to-size ratio, where the parameters are chosen such that the assumption, $\rho'_{\text{eff}} \leq 0$, is satisfied. For $\beta < -12.07$, we numerically find that the assumption is always violated. The first interesting example is found in the case, $\beta = -12.07$, in which the maximal mass-to-size ratio is obtained as $H_{\text{MAX}} = 1.018$ when $n_c/n_0 = 11.2$. This is a case that H_{MAX} exceeds the black hole limit, $H = 1$. Another interesting example is found in the case, $\beta = -11$, in which $H_{\text{MAX}} = 0.919$ when $n_c/n_0 = 11.3$. This is a case that H_{MAX} exceeds Buchdahl's limit, $H = 8/9 \approx 0.889$. These examples have academic importance in the sense that our analytic results in the previous section are partially realized also in the numerical solutions. However, when we impose a further physical assumption, $\rho - 3p \geq 0$, H_{MAX} never exceeds Buchdahl's limit as is seen in the 4th and 5th columns in Table 1. Note that the condition, $\beta < -5$, also excludes all the interesting cases in which H_{MAX} exceeds Buchdahl's limit.

Finally, let us find a critical value, $\beta_c < 0$, of β , such that, for $\beta < \beta_c$, nonlinear behaviors of the scalar field begin appearing. We numerically calculate a_s , b_s and c_s as functions of n_c for $\beta = -4, -5$ and -6 under the conditions, $\rho'_{\text{eff}} \leq 0$ and $\rho - 3p \geq 0$. We show (a_s, b_s) and c_s in Fig.11 and Fig.12, respectively. For $\beta \geq -4$, any deviation from general relativity is hardly seen. In the cases that $\beta = -5$ and -6 , these parameters show deviations from general relativity in which $a_s = b_s$ and $c_s = 0$. Our results are consistent with the previous works [6],[7], in which β_c is found to be -4.35 . Note that, even when $\beta < \beta_c$, our inequality, $|c_s| \leq 2\sqrt{3}/9$, is surely satisfied, which reconfirms our assertion that the nonlinear effects are always bounded in this sense.

5 Summary

We have derived a modified Buchdahl inequality in scalar-tensor theories of gravity. As a result, we have obtained two theory-independent inequalities, $b_s/\chi_s \leq 8/9$ and $|c_s/\chi_s| \leq 2\sqrt{3}/9$. The first inequality corresponds to the Buchdahl inequality in general relativity. The second inequality is characteristic to the scalar-tensor theories. Consequently, even if the scalar field is locally amplified due to non-perturbative effects in the strong gravitational field, a scalar mass, $-c/G_*$, is bounded in this sense.

The modified Buchdahl inequality is then reformulated to obtain a theory-dependent mass-to-size ratio, $2M/R$, with an example of the coupling function, $A(\varphi)$, in a simple form. If we take $\varphi_0 = 0$, the ADM mass in the physical frame is the same as that in general relativity, $M = b/2$. However, the physical radius, R , of the star can be smaller than the general relativistic one. As a result, the mass-to-size ratio can exceed not only Buchdahl's limit but also the black hole limit in contrast to general relativity.

Our analytic results have been numerically confirmed when we assume a polytropic equation of state for the matter. In particular, we have found the numerical solutions in which the mass-to-size ratio exceeds both Buchdahl's limit and the black hole limit. However, it has also been shown that these theoretically interesting stars would be unreal because of their unphysical

nature that $\rho - 3p$ becomes negative in the stars. Now suppose that a space rocket approaches a massive star such that $2M/R \gg 1$. If the rocket accidentally goes into a *Schwarzschild radius* of the star defined by $2M$, a spaceman in the rocket would be resigned to his fate to die. Now we know that, unfortunately for him, even if scalar-tensor theories well describe the classical gravity, he would hardly have a chance to return alive because he could hardly meet a real *false black hole*. He has the two possible futures, and both are equally tragic:

- If it is a black hole in general relativity, he can never escape.
- If it is a naked singularity in scalar-tensor theories, nobody knows what will happen when he touches it.

Acknowledgements

The authors would like to thank Dr. K. Oohara for useful discussion about numerical calculations.

A Observational constraints

In general, a coupling strength, $\alpha(\varphi)$, can be an arbitrary function of φ , and in the limit, $\alpha(\varphi) \rightarrow 0$, scalar-tensor theories approach general relativity. One defines

$$\alpha_0 \equiv \alpha(\varphi_0), \quad (A.1)$$

$$\beta_0 \equiv \left. \frac{d\alpha(\varphi)}{d\varphi} \right|_{\varphi=\varphi_0}, \quad (A.2)$$

where φ_0 is an asymptotic value of φ at spatial infinity. In the post-Newtonian approximation, the PPN parameters and the effective gravitational constant are expressed as follows [11]:

$$1 - \gamma_E = \frac{2\alpha_0^2}{1 + \alpha_0^2}, \quad (A.3)$$

$$\beta_E - 1 = \frac{\beta_0 \alpha_0^2}{2(1 + \alpha_0^2)^2}, \quad (A.4)$$

$$G = G_* A^2(\varphi_0) (1 + \alpha^2(\varphi_0)). \quad (A.5)$$

General relativity corresponds to the case that $\beta_E = \gamma_E = 1$ [4],[14]. Experiments on the time delay and deflection of light in the solar system constrain $|1 - \gamma_E|$ as [12]

$$|1 - \gamma_E| < 2 \times 10^{-3}, \quad (A.6)$$

which constrains $\omega(\phi)$ and α_0 as

$$\omega > 500, \quad \alpha_0^2 < 10^{-3}. \quad (A.7)$$

The lunar-laser-ranging experiments constrain $|\beta_E - 1|$ as [12]

$$|\beta_E - 1| \lesssim 6 \times 10^{-4}, \quad (A.8)$$

which constrains some combination of α_0 and β_0 , only. Consequently, if α_0 tends toward zero, the constraint on β_0 is effectively lost. However, another constraint on β_0 is obtained from observations of the binary-pulsars, PSR1913+16, as [7],[12]

$$\beta_0 > -5. \quad (\text{A.9})$$

When we take (3.40) as a coupling function, the coupling strength is $\alpha(\varphi) = \beta\varphi$. Accordingly, $\alpha_0 = \beta\varphi_0$, and we obtain the constraint on φ_0 . In this paper we take $\varphi_0 = 0$ for simplicity.

B An exterior solution

A line element of the unphysical frame in the Just coordinate is [15]

$$ds_* = -e^{\gamma(\chi)}dt^2 + e^{-\gamma(\chi)}d\chi^2 + e^{\lambda(\chi)-\gamma(\chi)}d\Omega^2. \quad (\text{B.1})$$

The field equations in the exterior space-time are the following:

$$\gamma'' + \gamma'\lambda' = 0, \quad (\text{B.2})$$

$$-\gamma'^2 + \gamma'\lambda' - \lambda'^2 + \gamma'' - 2\lambda'' = 4\varphi'^2, \quad (\text{B.3})$$

$$2 + e^\lambda(\gamma'\lambda' - \lambda'^2 + \gamma'' - \lambda'') = 0, \quad (\text{B.4})$$

$$\varphi'' + \lambda'\varphi' = 0, \quad (\text{B.5})$$

where a prime denotes a derivative with respect to χ . With (B.2),(B.4) and (B.5), the exterior solution can be obtained as

$$e^{\lambda(\chi)} = \chi^2 - a\chi, \quad (\text{B.6})$$

$$e^{\gamma(\chi)} = \left(1 - \frac{a}{\chi}\right)^{\frac{b}{a}}, \quad (\text{B.7})$$

$$\varphi(\chi) = \varphi_0 + \frac{c}{a} \ln \left(1 - \frac{a}{\chi}\right), \quad (\text{B.8})$$

where a, b and c are constants of integration, and φ_0 denotes an asymptotic value of φ at infinity. With (B.3), one finds

$$a^2 - b^2 = 4c^2. \quad (\text{B.9})$$

The coordinate transformation between the Schwarzschild coordinate, r , and the Just coordinate, χ , is given by

$$r^2 = \chi^2 \left(1 - \frac{a}{\chi}\right)^{\frac{a-b}{a}}. \quad (\text{B.10})$$

Note that $r \rightarrow \chi$ at spatial infinity. In the Schwarzschild coordinate, a line element becomes

$$ds_*^2 = -e^{2\nu(r)}dt^2 + e^{2\mu(r)}dr^2 + r^2d\Omega^2. \quad (\text{B.11})$$

The exterior solution in the Schwarzschild coordinate is given by

$$e^{2\nu(r)} = \left(1 - \frac{a}{\chi(r)}\right)^{\frac{b}{a}}, \quad (\text{B.12})$$

$$e^{2\mu(r)} = \left(1 - \frac{a}{\chi(r)}\right) \left(1 - \frac{a+b}{2\chi(r)}\right)^{-2}. \quad (\text{B.13})$$

Asymptotic behaviors of the exterior solution at spatial infinity are as follows:

$$e^{2\nu(r)} \longrightarrow 1 - \frac{b}{r}, \quad (\text{B.14})$$

$$e^{2\mu(r)} \longrightarrow 1 + \frac{b}{r}, \quad (\text{B.15})$$

$$\varphi(r) \longrightarrow \varphi_0 - \frac{c}{r}. \quad (\text{B.16})$$

Hence, we can interpret b and c as, respectively, a tensor mass, $M_T = b/2G_*$, and a scalar mass, $M_S = -c/G_*$, in the unphysical frame.

C An interior solution: Numerical methods

Using variables, $m_*(r)$ and $\nu(r)$, defined by

$$f_*(r) \equiv e^{2\nu(r)}, \quad h_*(r) \equiv \left[1 - \frac{2m_*(r)}{r}\right]^{-1}, \quad (\text{C.1})$$

the field equations (3.6) \sim (3.9) become

$$\frac{dm_*}{dr} = 4\pi G_* A^4(\varphi) r^2 \rho + \frac{1}{2} r(r - 2m_*) \psi^2, \quad (\text{C.2})$$

$$\frac{d\nu}{dr} = \frac{m_* + 4\pi G_* A^4(\varphi) r^3 p}{r(r - 2m_*)} + \frac{1}{2} r \psi^2 \equiv \Phi(r), \quad (\text{C.3})$$

$$\frac{d\varphi}{dr} = \psi, \quad (\text{C.4})$$

$$\frac{d\psi}{dr} = \frac{4\pi G_* A^4(\varphi) r}{r - 2m_*} [\alpha(\varphi)(\rho - 3p) + (\rho - p)r\psi] - \frac{2(r - m_*)}{r(r - 2m_*)}\psi, \quad (\text{C.5})$$

$$\frac{dp}{dr} = -(\rho + p)(\Phi + \alpha(\varphi)\psi). \quad (\text{C.6})$$

The total baryon mass measured in the physical frame is

$$\bar{m} = m_b \int n\sqrt{-g}u^0 d^3x = m_b \int_0^{r_s} 4\pi n A^3(\varphi) r^2 \left(1 - \frac{2m_*}{r}\right)^{-\frac{1}{2}} dr. \quad (\text{C.7})$$

Given the equation of state, we can numerically integrate the above field equations outward from the center, $r = 0$, with the boundary conditions as follows:

$$\left. \begin{aligned} m_*(0) &= 0, \\ \varphi(0) &= \varphi_c, \\ \psi(0) &= 0, \\ p(0) &= p_c, \\ \rho(0) &= \rho_c, \end{aligned} \right\} \quad (\text{C.8})$$

where ρ_c and p_c are given by replacing n in (4.1) and (4.2) with $n_c \equiv n(0)$. A surface of the star, $r = r_s$, is determined by the condition, $p(r_s) = 0$. A numerically obtained interior solution is to be matched to the exterior one by the conditions [6],[7],

$$\varphi_0 = \varphi_s + \frac{\psi_s}{\sqrt{\nu'_s{}^2 + \psi_s{}^2}} \tanh^{-1} \left(\frac{\sqrt{\nu'_s{}^2 + \psi_s{}^2}}{\nu'_s + 1/r_s} \right), \quad (\text{C.9})$$

$$b = 2r_s{}^2 \nu'_s \sqrt{1 - \frac{2m_{*s}}{r_s}} \exp \left(-\frac{\nu'_s}{\sqrt{\nu'_s{}^2 + \psi_s{}^2}} \tanh^{-1} \left(\frac{\sqrt{\nu'_s{}^2 + \psi_s{}^2}}{\nu'_s + 1/r_s} \right) \right), \quad (\text{C.10})$$

$$c = \frac{\psi_s}{2\nu'_s} b, \quad (\text{C.11})$$

$$a = \sqrt{b^2 + 4c^2}, \quad (\text{C.12})$$

where a prime denotes a derivative with respect to r , and a subscript, s , refers to quantities evaluated at the surface, r_s . A central value of φ , φ_c , is chosen such that we have $\varphi_0 = 0$.

References

- [1] C. Brans and R. H. Dicke, Phys. Rev. **124**, 925 (1962).
- [2] P. G. Bergmann, Int. J. Theor. Phys. **1**, 25 (1968).
- [3] R. V. Wagoner, Phys. Rev. **D1**, 3209, (1970).
- [4] C. M. Will, *Theory and Experiment in Gravitational Physics*, (Cambridge University Press, Cambridge, 1993).
- [5] M. B. Green, J. H. Schwartz and E. Witten, *Superstring Theory vols. 1,2*, (Cambridge University Press, Cambridge, 1987).
- [6] T. Damour and G. Esposito-Farèse, Phys. Rev. Lett. **70**, 2220 (1993).
- [7] T. Damour and G. Esposito-Farèse, *preprint* gr-qc/9602056.
- [8] H. A. Buchdahl, Phys. Rev. **116**, 1027 (1959).
- [9] S. Weinberg, *Gravitation and Cosmology*, (Wiley, New York, 1972).
- [10] R. M. Wald, *General Relativity*, (The University of Chicago Press, Chicago and London, 1984).
- [11] T. Chiba, T. Harada and K. Nakao, Prog. Theor. Phys. Suppl. **128**, 335 (1997).
- [12] G. Esposito-Farèse, *preprint* gr-qc/9612039.
- [13] S. L. Shapiro and S. A. Teukolsky, *Black Holes, White Dwarfs and Neutron Stars*, (Wiley, 1983).
- [14] C. W. Misner, K. S. Thorne and J. A. Wheeler, *Gravitation*, (Freeman, San Francisco, 1973).
- [15] T. Damour and G. Esposito-Farèse, Class. Quant. Grav. **9**, 2093 (1992).

Figure 1: The allowed region, D , is depicted, where horizontal and vertical axes denote, respectively, b_s and a_s . The characteristic points, $P = (4(3 - 2\sqrt{2}), 4(3\sqrt{2} - 4))$, $Q = (8/9, 8/9)$ and $K = (4/9, 8/9)$, are shown. In general relativity, $a_s = b_s$. Buchdahl's limit is denoted by Q . On K , $|c_s|$ takes the maximum value, $|c_s|_{\text{MAX}} = 2\sqrt{3}/9$.

Figure 2: On each lines, $H(a_s, b_s; \beta) = 8/9$ for various values of β : $0, -3, -5, -10$ and -100 . Horizontal and vertical axes denote, respectively, b_s and a_s .

Figure 3: The Maximum mass-to-size ratio, H_{MAX} , is shown as a function of β . Horizontal and vertical axes denote, respectively, β , and H_{MAX} . A horizontal line, $H_{\text{MAX}} = 8/9$, denotes Buchdahl's limit in general relativity. When $\beta \lesssim 0.4$, H_{MAX} exceeds Buchdahl's limit. When $\beta \lesssim 0.2$, H_{MAX} exceeds unity, a black hole limit.

Figure 4: The effective density, $\rho_{\text{eff}}(r)$, is shown in the case that $\beta = -5$ and $n_c/n_0 = 10$. Horizontal and vertical axes denote, respectively, the radial coordinate, r , in the unit of 10km, and the effective density, $\rho_{\text{eff}}(r)/(m_b n_0)$. It is seen that the assumption, $\rho'_{\text{eff}}(r) \leq 0$, is satisfied.

Figure 5: Each term of (4.5) in $\rho'_{\text{eff}}(r)$ is shown for $\beta = -5$ and $n_c/n_0 = 10$. Horizontal and vertical axes denote, respectively, the radial coordinate, r , in the unit of 10km, and the 1st, 2nd and 3rd terms in (4.5).

Figure 6: We compare $\phi(r)$, $\rho(r)$ and $\varphi(r)$ in the case that $\beta = -5$ and $n_c/n_0 = 7.9$. Horizontal and vertical axes denote, respectively, the radial coordinate, r , in the unit of 10km, and $\rho(r)/(m_b n_0)$, $\phi(r)$ and $\varphi(r)$. On a thin dotted line, $G \equiv 1/\phi_0 = 1$, i.e., general relativity.

Figure 7: The effective density, $\rho_{\text{eff}}(r)$, is shown in the case that $\beta = -30$ and $n_c/n_0 = 10$. Horizontal and vertical axes denote, respectively, the radial coordinate, r , in the unit of 10km, and the effective density, $\rho_{\text{eff}}(r)/(m_b n_0)$. It is seen that the assumption, $\rho'_{\text{eff}}(r) \leq 0$, is partially violated between two rectangles.

Figure 8: Each term of (4.5) in $\rho'_{\text{eff}}(r)$ is shown for $\beta = -30$ and $n_c/n_0 = 10$. Horizontal and vertical axes denote, respectively, the radial coordinate, r , in the unit of 10km, and the 1st, 2nd and 3rd terms in (4.5).

Figure 9: We compare $\phi(r)$, $\rho(r)$ and $\varphi(r)$ in the case that $\beta = -30$ and $n_c/n_0 = 10$. Horizontal and vertical axes denote, respectively, the radial coordinate, r , in the unit of 10km, and $\rho(r)/(m_b n_0)$, $\phi(r)$ and $\varphi(r)$. On a thin dotted line, $G \equiv 1/\phi_0 = 1$, i.e., general relativity.

Figure 10: We show $\rho(r)$ and $p(r)$ in the physical frame for $\beta = -30$ and $n_c/n_0 = 10$. Horizontal and vertical axes denote, respectively, the radial coordinate, r , in the unit of 10km, and $\rho(r)/(m_b n_0)$ and $p(r)/(m_b n_0)$. Though the assumption, $\rho'_{\text{eff}}(r) \leq 0$, is violated in the unphysical frame, the conditions, $\rho(r) - 3p(r) \geq 0$, $\rho'(r) \leq 0$ and $p'(r) \leq 0$ are all satisfied in the physical frame.

Figure 11: We show the parameters, (a_s, b_s) , in each equilibrium solution for $n_c/n_0 = 2.5 \sim 10.3$. We take $\beta = -4, -5$ and -6 , and impose the conditions, $\rho(r) - 3p(r) \geq 0$ and $\rho'_{\text{eff}}(r) \leq 0$. Horizontal and vertical axes denote, respectively, b_s and a_s .

Figure 12: We show the parameter, c_s , in each equilibrium solution for $n_c/n_0 = 1.0 \sim 10.3$. We take $\beta = -4, -5$ and -6 , and impose the conditions, $\rho(r) - 3p(r) \geq 0$ and $\rho'_{\text{eff}}(r) \leq 0$. Horizontal and vertical axes denote, respectively, n_c/n_0 and c_s . A horizontal thin dotted line denotes the limit on c_s , i.e., $c_s = -2\sqrt{3}/9$.

| β | n_c/n_0 | $\rho'_{\text{eff}} \leq 0$ | $\rho - 3p \geq 0$ | H_{max} |
|---------|-------------|-----------------------------|--------------------|------------------|
| -12.07 | 0.1 ~ 10.3 | ○ | ○ | 0.679 |
| | 10.3 ~ 11.2 | ○ | ✗ | 1.018 |
| -11.0 | 0.1 ~ 10.3 | ○ | ○ | 0.666 |
| | 10.3 ~ 11.3 | ○ | ✗ | 0.919 |
| -10.0 | 0.1 ~ 10.3 | ○ | ○ | 0.651 |
| | 10.3 ~ 11.4 | ○ | ✗ | 0.834 |
| -6.0 | 0.1 ~ 10.3 | ○ | ○ | 0.556 |
| | 10.3 ~ 11.2 | ○ | ✗ | 0.569 |
| -5.0 | 0.1 ~ 10.3 | ○ | ○ | 0.517 |
| | 10.3 ~ 15.7 | ○ | ✗ | 0.567 |
| -4.0 | 0.1 ~ 10.3 | ○ | ○ | 0.514 |
| | 10.3 ~ 14.9 | ○ | ✗ | 0.562 |
| 0.0 | 0.1 ~ 10.3 | ○ | ○ | 0.514 |
| | 10.3 ~ 14.9 | ○ | ✗ | 0.562 |

Table 1: We summarize our numerical results. In the 1st column, β is given. In the 2nd column, we show a range of n_c in our numerical researches. In the 3rd and 4th column, we show, respectively, whether the assumption, $\rho'_{\text{eff}} \leq 0$, and the condition, $\rho - 3p \geq 0$, are satisfied. In the 5th column, the maximum mass-to-size ratio is shown for each β .

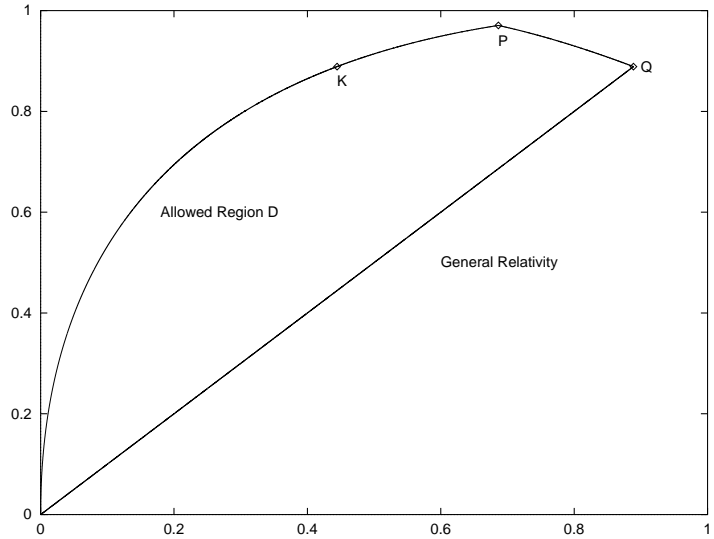


Figure 1: The allowed region, D , is depicted, where horizontal and vertical axes denote, respectively, b_s and a_s . The characteristic points, $P = (4(3 - 2\sqrt{2}), 4(3\sqrt{2} - 4))$, $Q = (8/9, 8/9)$ and $K = (4/9, 8/9)$, are shown. In general relativity, $a_s = b_s$. Buchdahl's limit is denoted by Q . On K , $|c_s|$ takes the maximum value, $|c_s|_{\text{MAX}} = 2\sqrt{3}/9$.

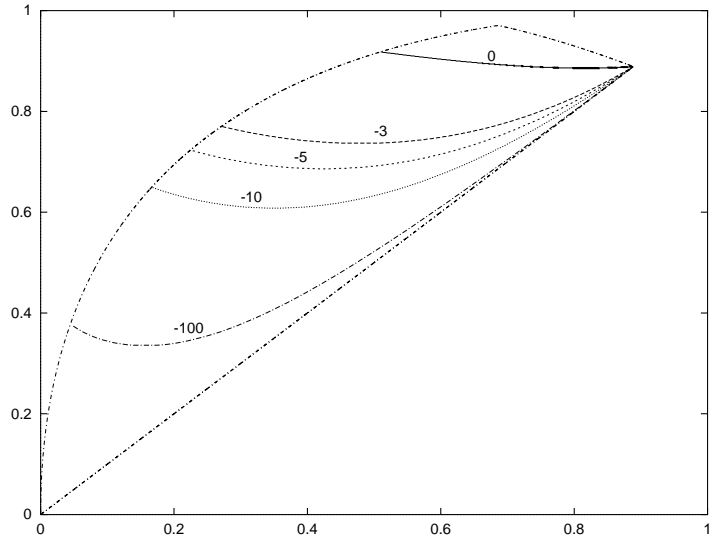


Figure 2: On each lines, $H(a_s, b_s; \beta) = 8/9$ for various values of β : $0, -3, -5, -10$ and -100 . Horizontal and vertical axes denote, respectively, b_s and a_s .

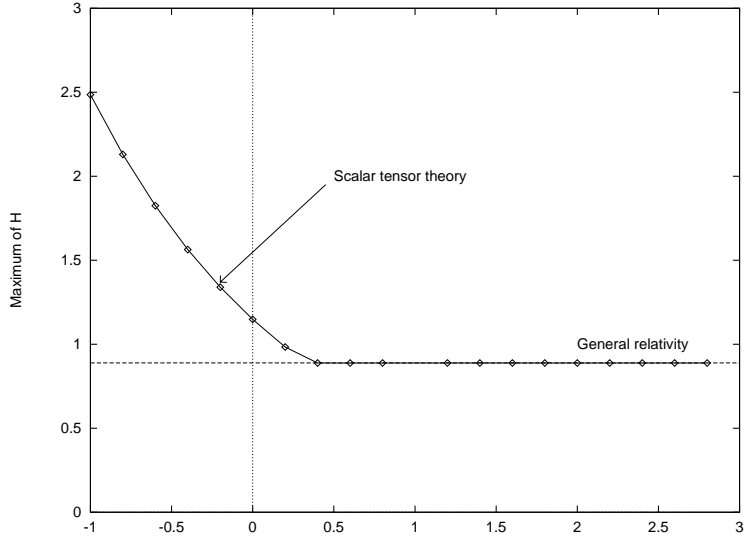


Figure 3: The Maximum mass-to-size ratio, H_{MAX} , is shown as a function of β . Horizontal and vertical axes denote, respectively, β , and H_{MAX} . A horizontal line, $H_{\text{MAX}} = 8/9$, denotes Buchdahl's limit in general relativity. When $\beta \lesssim 0.4$, H_{MAX} exceeds Buchdahl's limit. When $\beta \lesssim 0.2$, H_{MAX} exceeds unity, a black hole limit.

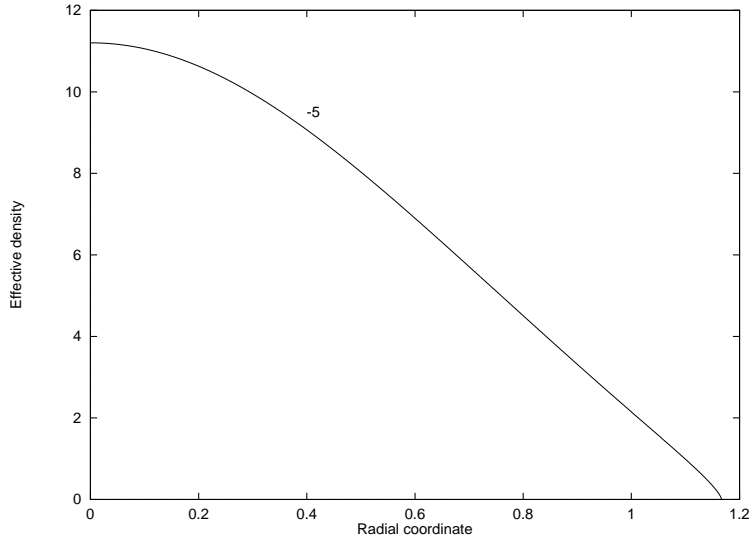


Figure 4: The effective density, $\rho_{\text{eff}}(r)$, is shown in the case that $\beta = -5$ and $n_c/n_0 = 10$. Horizontal and vertical axes denote, respectively, the radial coordinate, r , in the unit of 10km, and the effective density, $\rho_{\text{eff}}(r)/(m_b n_0)$. It is seen that the assumption, $\rho'_{\text{eff}}(r) \leq 0$, is satisfied.

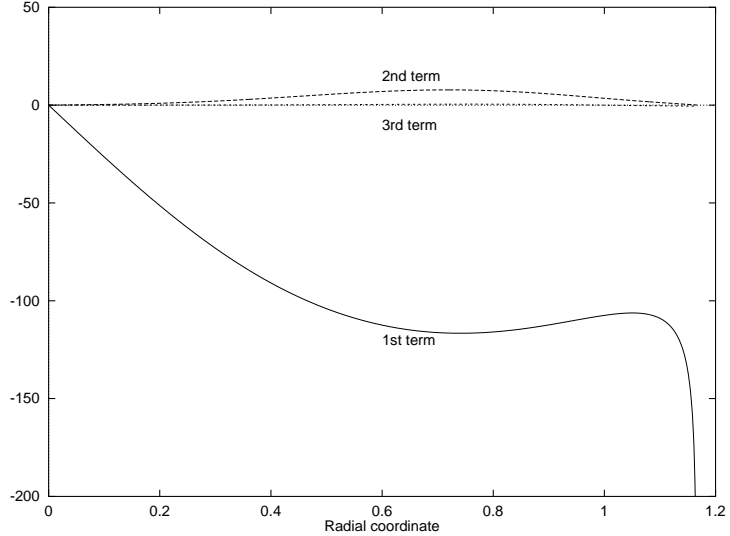


Figure 5: Each term of (4.5) in $\rho'_{\text{eff}}(r)$ is shown for $\beta = -5$ and $n_c/n_0 = 10$. Horizontal and vertical axes denote, respectively, the radial coordinate, r , in the unit of 10km, and the 1st, 2nd and 3rd terms in (4.5).

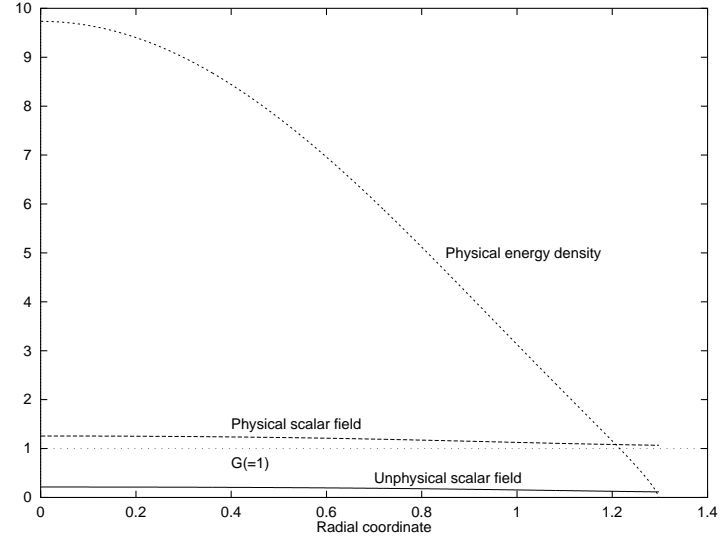


Figure 6: We compare $\phi(r)$, $\rho(r)$ and $\varphi(r)$ in the case that $\beta = -5$ and $n_c/n_0 = 7.9$. Horizontal and vertical axes denote, respectively, the radial coordinate, r , in the unit of 10km, and $\rho(r)/(m_b n_0)$, $\phi(r)$ and $\varphi(r)$. On a thin dotted line, $G \equiv 1/\phi_0 = 1$, i.e., general relativity.

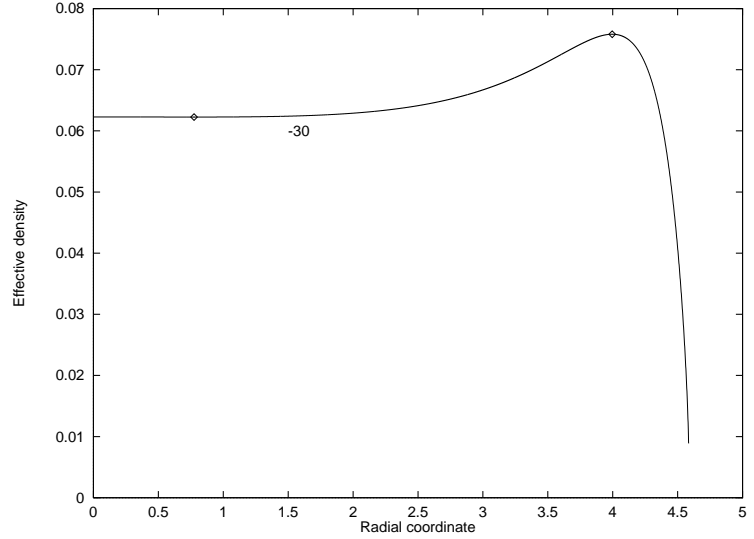


Figure 7: The effective density, $\rho_{\text{eff}}(r)$, is shown in the case that $\beta = -30$ and $n_c/n_0 = 10$. Horizontal and vertical axes denote, respectively, the radial coordinate, r , in the unit of 10km, and the effective density, $\rho_{\text{eff}}(r)/(m_b n_0)$. It is seen that the assumption, $\rho'_{\text{eff}}(r) \leq 0$, is partially violated between two rectangles.

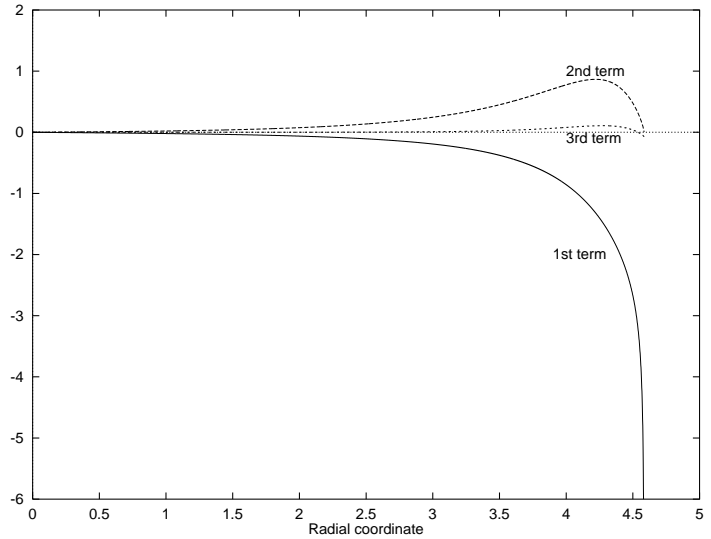


Figure 8: Each term of (4.5) in $\rho'_{\text{eff}}(r)$ is shown for $\beta = -30$ and $n_c/n_0 = 10$. Horizontal and vertical axes denote, respectively, the radial coordinate, r , in the unit of 10km, and the 1st, 2nd and 3rd terms in (4.5).

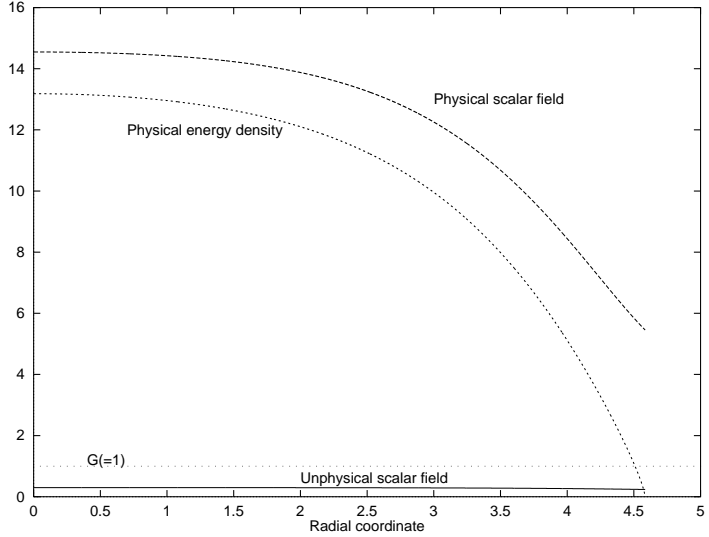


Figure 9: We compare $\phi(r)$, $\rho(r)$ and $\varphi(r)$ in the case that $\beta = -30$ and $n_c/n_0 = 10$. Horizontal and vertical axes denote, respectively, the radial coordinate, r , in the unit of 10km, and $\rho(r)/(m_b n_0)$, $\phi(r)$ and $\varphi(r)$. On a thin dotted line, $G \equiv 1/\phi_0 = 1$, i.e., general relativity.

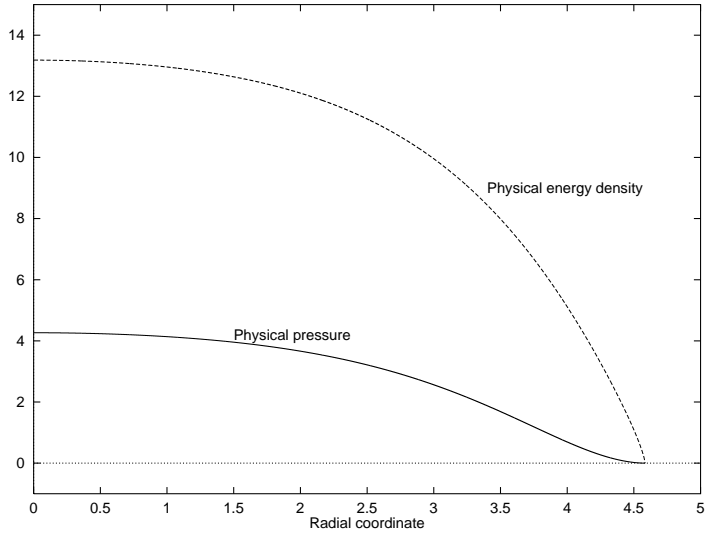


Figure 10: We show $\rho(r)$ and $p(r)$ in the physical frame for $\beta = -30$ and $n_c/n_0 = 10$. Horizontal and vertical axes denote, respectively, the radial coordinate, r , in the unit of 10km, and $\rho(r)/(m_b n_0)$ and $p(r)/(m_b n_0)$. Though the assumption, $\rho'_{\text{eff}}(r) \leq 0$, is violated in the unphysical frame, the conditions, $\rho(r) - 3p(r) \geq 0$, $\rho'(r) \leq 0$ and $p'(r) \leq 0$ are all satisfied in the physical frame.

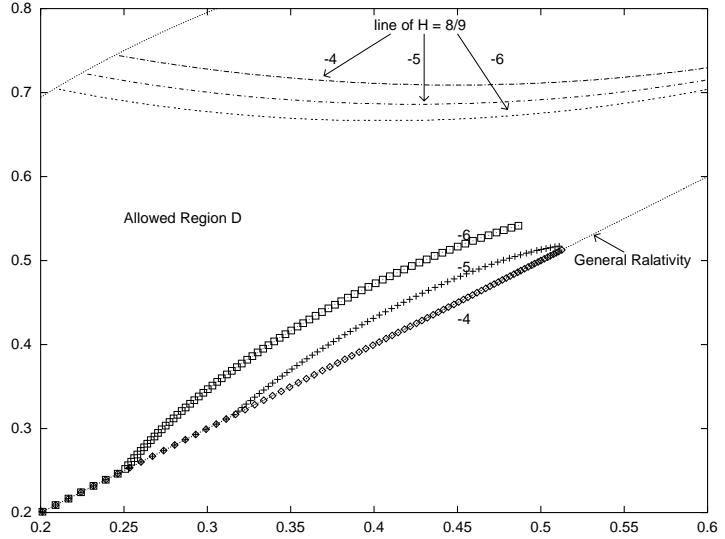


Figure 11: We show the parameters, (a_s, b_s) , in each equilibrium solution for $n_c/n_0 = 2.5 \sim 10.3$. We take $\beta = -4, -5$ and -6 , and impose the conditions, $\rho(r) - 3p(r) \geq 0$ and $\rho'_{\text{eff}}(r) \leq 0$. Horizontal and vertical axes denote, respectively, b_s and a_s .

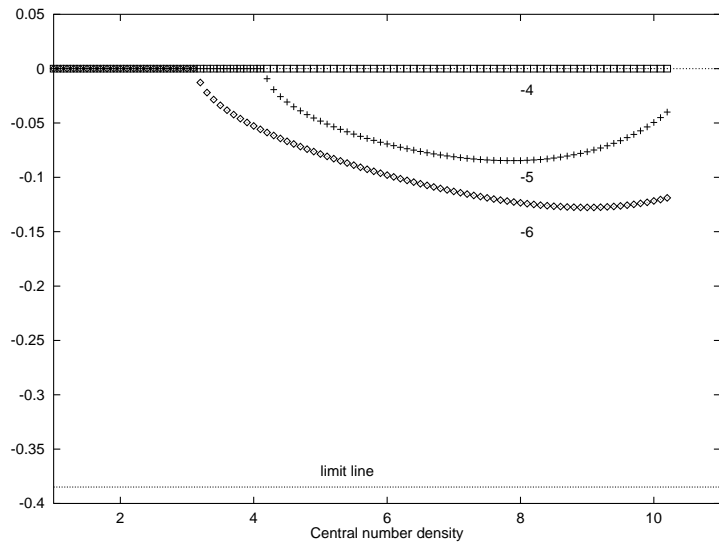


Figure 12: We show the parameter, c_s , in each equilibrium solution for $n_c/n_0 = 1.0 \sim 10.3$. We take $\beta = -4, -5$ and -6 , and impose the conditions, $\rho(r) - 3p(r) \geq 0$ and $\rho'_{\text{eff}}(r) \leq 0$. Horizontal and vertical axes denote, respectively, n_c/n_0 and c_s . A horizontal thin dotted line denotes the limit on c_s , i.e., $c_s = -2\sqrt{3}/9$.

| β | n_c/n_0 | $\rho'_{\text{eff}} \leq 0$ | $\rho - 3p \geq 0$ | H_{max} |
|---------|-------------|-----------------------------|--------------------|------------------|
| -12.07 | 0.1 ~ 10.3 | ○ | ○ | 0.679 |
| | 10.3 ~ 11.2 | ○ | ✗ | 1.018 |
| -11.0 | 0.1 ~ 10.3 | ○ | ○ | 0.666 |
| | 10.3 ~ 11.3 | ○ | ✗ | 0.919 |
| -10.0 | 0.1 ~ 10.3 | ○ | ○ | 0.651 |
| | 10.3 ~ 11.4 | ○ | ✗ | 0.834 |
| -6.0 | 0.1 ~ 10.3 | ○ | ○ | 0.556 |
| | 10.3 ~ 11.2 | ○ | ✗ | 0.569 |
| -5.0 | 0.1 ~ 10.3 | ○ | ○ | 0.517 |
| | 10.3 ~ 15.7 | ○ | ✗ | 0.567 |
| -4.0 | 0.1 ~ 10.3 | ○ | ○ | 0.514 |
| | 10.3 ~ 14.9 | ○ | ✗ | 0.562 |
| 0.0 | 0.1 ~ 10.3 | ○ | ○ | 0.514 |
| | 10.3 ~ 14.9 | ○ | ✗ | 0.562 |

Table 1: We summarize our numerical results. In the 1st column, β is given. In the 2nd column, we show a range of n_c in our numerical researches. In the 3rd and 4th column, we show, respectively, whether the assumption, $\rho'_{\text{eff}} \leq 0$, and the condition, $\rho - 3p \geq 0$, are satisfied. In the 5th column, the maximum mass-to-size ratio is shown for each β .

